MEASUREMENTS OF THE PHOTOEMISSION SPECTRA OF OXYGEN-FREE AND OXYGEN-DOPED *p*-TERPHENYL SINGLE CRYSTALS IN THE VACUUM UV REGION

MINORU HISA

Department of Physics, Faculty of Education, Wakayama University, Wakayama 640 (Japan)

KATSUJI HIGASHINO

Science Education Institute of Sakai City, Sakai 591 (Japan)

TAKANORI OSHIO

Research Institute for Atomic Energy, Osaka City University, Osaka 558 (Japan)

(Received March 9, 1982; in revised form April 20, 1982)

Summary

The energy distribution curves (EDCs) and photoemission yield curves (PYCs) of electrons photoemitted from oxygen-free and oxygen-doped *p*-terphenyl single crystals were measured in the photon energy range 6.0 - 10.3 eV. The oxygen impurities acted both to suppress (via ejection of electrons from the valence bands and impurity levels) and to enhance (via relaxation processes such as the Auger effect) photoemission. The first and second onset energies of electron ejection were estimated from the PYC spectra to be about 6.9 eV and 7.7 eV respectively. New peaks which depended on electron relaxation rather than electron ejection appeared in the low kinetic energy region of the EDC spectra. The presence of oxygen impurities leads to a reduction in the threshold energies of photoemission and in the quantum yield of photoemission from the crystal surface. The oxygen impurities also affect the electronic potential energy of the valence bands.

1. Introduction

The measurement of an external photoelectric effect [1, 2] is a very useful method of investigating the electronic structure of solids. Energy distribution curves (EDCs) and photoemission yield curves (PYCs) provide much helpful information on electronic energy states and on the conversion of electron energy in solids. Photoelectron spectra have been measured using several different methods [1, 2].

0047-2670/82/0000-0000/$02.75

Photoemission from anthracene, naphthacene, chrysene etc. has been investigated from the beginning of the 1960s [3 - 5]. Hino *et al.* [6] have measured EDCs and PYCs for *p*-terphenyl crystals. Geacintov and Pope [7] and Zagrubskii and Viesov [8] obtained evidence for the presence of an autoionization process by the detailed analysis of EDC and PYC data from anthracene, naphthacene and other organic crystals. Kochi *et al.* [9] have discussed the effect of electron ejection on photoemission from many aromatic compounds. They concluded that the electron energy loss could be attributed to the production of secondary electrons. Seki *et al.* [10] proposed that excitons and electron pairs were created in the photoemission process. Ueno *et al.* [11] used a low energy electron diffraction method to demonstrate that the above conditions existed in organic crystals. Thus the application of either of these methods is effective in the analysis of the electronic structure of *p*-terphenyl.

There have been few investigations of the effect of organic impurities on electron energy losses in external photoelectric effects in the vacuum UV region. The purpose of the present work is to determine the effect of oxygen impurities on the photoemission spectrum of a *p*-terphenyl single crystal. Therefore the EDCs and PYCs of both oxygen-free (crystal A) and oxygen-doped (crystal B) *p*-terphenyl single crystals were investigated.

2. Experimental details

Recrystallized *p*-terphenyl was purified by 200 pass zone refining. The oxygen-free crystals A were grown in a nitrogen atmosphere using the Bridgman method. The oxygen-doped crystals B were grown from benzene solutions saturated with oxygen gas and were kept in a vacuum for 1 h at room temperature in order to remove the solvent from the crystals. Each crystal had a cross section of 5 mm $\times$ 10 mm and was about 60 μm thick.

A block diagram of the experimental arrangement is shown in Fig. 1. A hydrogen capillary discharge tube of the type described by Newburgh *et al.* [12] was used as the light source and was operated under glow discharge conditions with a d.c. current of 450 mA, an applied voltage of 3 kV and a flowing hydrogen gas pressure of about 1 Torr. The light was passed through a 0.5 m Seya–Namioka vacuum UV monochromator (Shimazu Inc. model SGV-50) equipped with a platinum-coated concave grating (Bausch and Lomb) with 1200 grooves mm^{-1}. In order to eliminate the superposition of higher order spectra in the continuum spectrum region of hydrogen, a synthetic fused quartz or CaF filter was placed in front of the double-beam splitter.

The output light was measured using an end-on photomultiplier tube with a sodium-salicylate-coated glass plate attached to the front. The quantum yield of sodium salicylate fluorescence is approximately constant over the wavelength range 1200 - 2000 Å [13]. Since sodium salicylate is dissociated by irradiation with vacuum UV radiation for more than 3 h, the

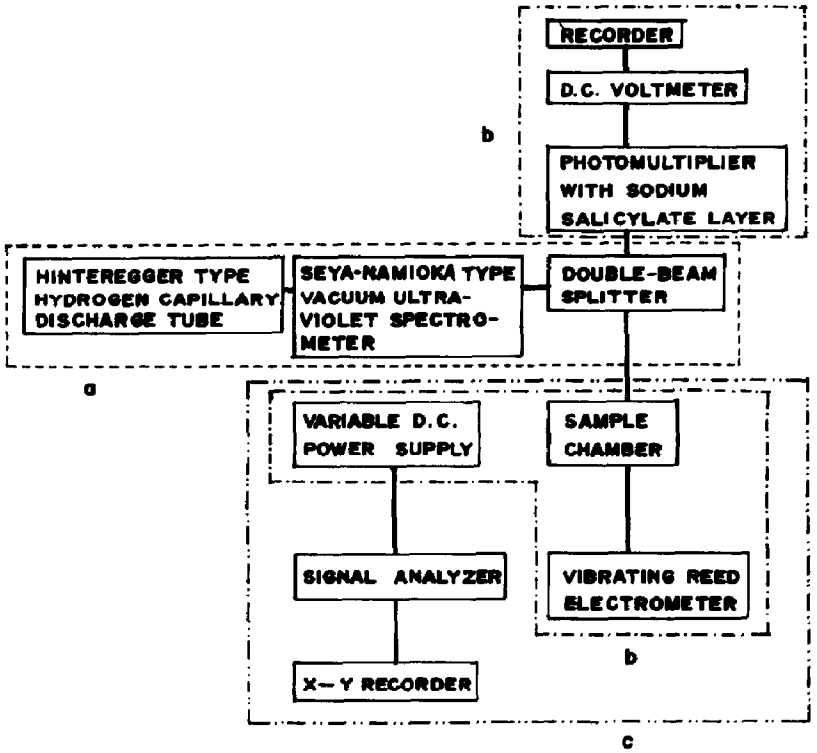

Fig. 1. Experimental arrangement for measuring the PYCs and EDCs: blocks a, b and c were used to measure the PYCs; blocks a and c were used to measure the EDCs.

duration of the measurements was not allowed to exceed 2 h and fresh sodium salicylate was used for each measurement. The absolute light intensities were determined from the angular distribution of the fluorescence [14] and the absolute quantum yield of the sodium salicylate fluorescence which was calibrated using a double-ionization chamber [15].

The absorption spectra were measured in order to investigate the electronic interband transitions in the photoemission processes. The photoemission spectra were measured using an instrument equipped with a cylindrical collector can similar to that employed by Krolikowski [16] and James *et al.* [17] (Fig. 2). The light beam was incident at an angle of 90° to the *ab* plane of the crystal in all the measurements.

If a retarding voltage V is applied to the collector of this instrument the photoelectric current $I(V)$ is given by

$$I(V) = \frac{2}{\pi} \int_{eV}^{E_m} dE_k \int_0^{\pi/2} \cos\phi \, d\phi \int_0^{\pi/2} eI_0(E_k, \phi, \theta) \, d\theta \tag{1}$$

where E_k and E_m are the kinetic energy and the maximum kinetic energy of the emitted photoelectrons respectively, $I_0(E_k, \phi, \theta)$ is the distribution function of the photoelectron intensity, θ is the angle between the direction of the emitted electrons and the core axis and ϕ is the angle between the

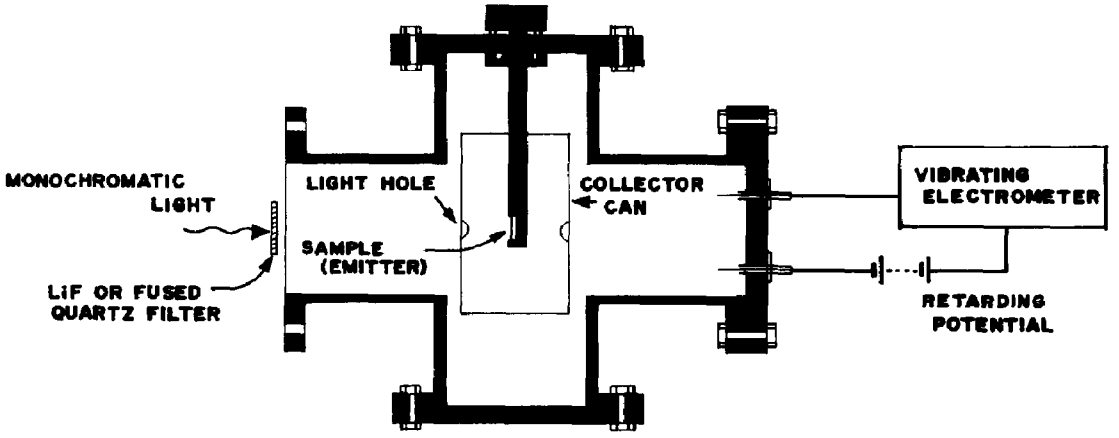

(a)

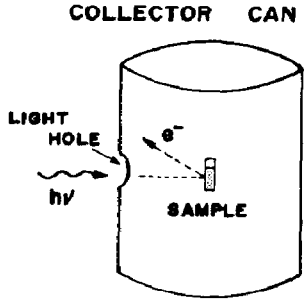

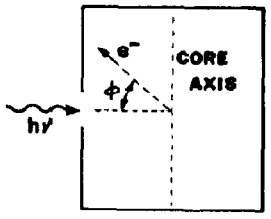

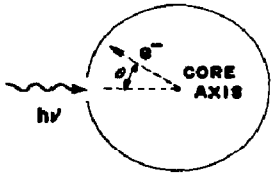

(b)

Fig. 2. (a) Cross-sectional view of the cylindrical sample chamber; (b) collector can and the directions of the emitted photoelectrons (θ, angle between the direction of the emitted electrons and the core axis; ϕ, the angle between the direction of the emitted photoelectrons and the radial direction of the collector can).

direction of the emitted photoelectrons and the radial direction of the collector can (see Fig. 2(a)). Differentiation of eqn. (1) with respect to a retarding potential V gives

$$\frac{dI}{dV} = -\int_{eV}^{E_m} \frac{eI_0(E_k)}{2E_k(1-eV/E_k)^{1/2}}\, dE_k \tag{2}$$

EDCs calculated using eqn. (2) are shown in Figs. 3(c) and 4(c). The resolution limit of the EDC peaks was estimated as 0.2 eV by an analysis of the reproducibility of the EDC spectra in the present measurements.

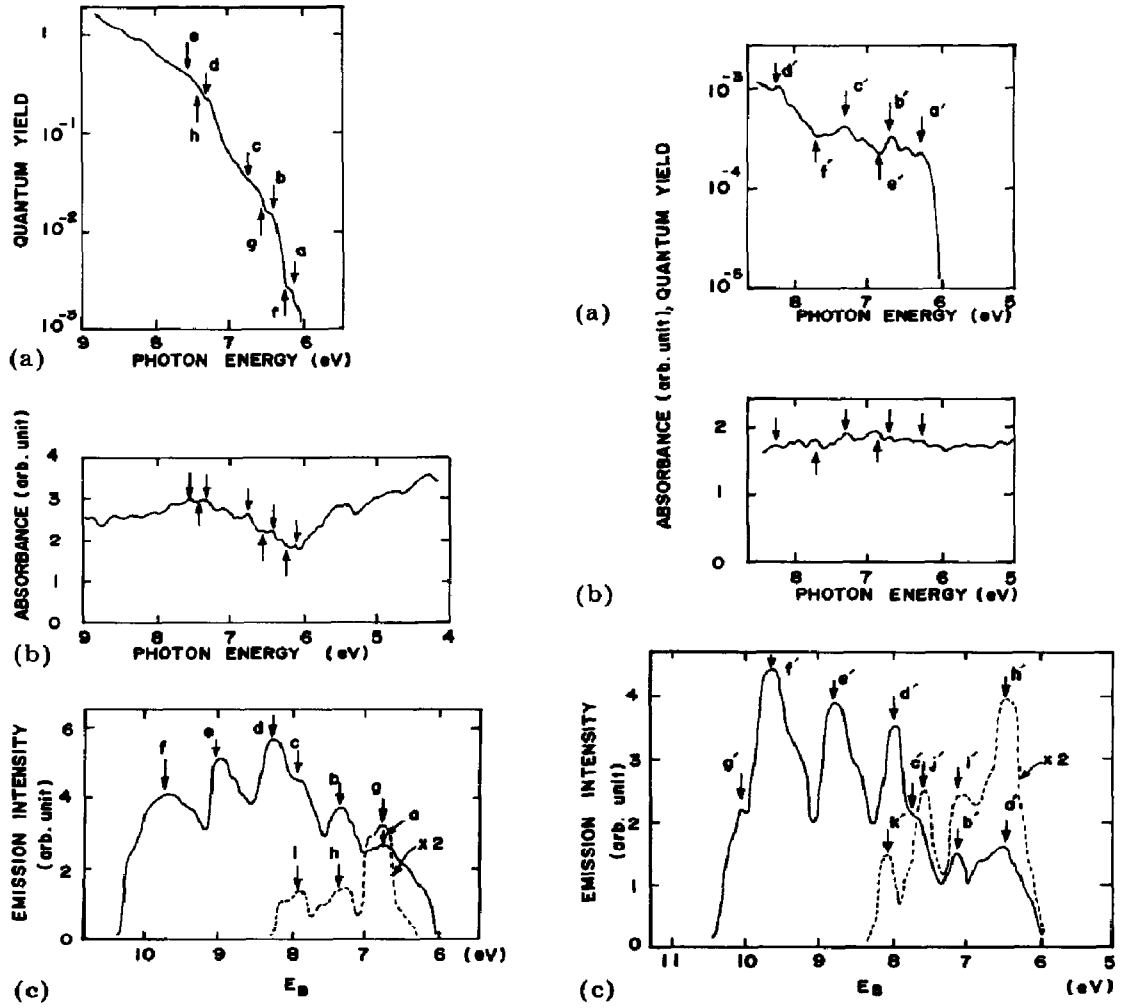

Fig. 3. Photoemission and absorption spectra of crystal A: (a) PYC; (b) absorption spectrum; (c) EDC (— — —, $h\nu$ = 7.65 eV; ——, $h\nu$ = 10.2 eV).

Fig. 4. Photoemission and absorption spectra of crystal B: (a) PYC; (b) absorption spectrum; (c) EDC (— — —, $h\nu$ = 7.65 eV; ——, $h\nu$ = 10.2 eV).

3. Results

3.1. Photoelectric yield curve

Figures 3(b) and 4(b) show the absorption spectra of the crystals A and B respectively. Comparison of Figs. 3(a) and 4(a) shows that the quantum yield of photoelectrons emitted from the surface of crystal B is smaller by a factor of 100 than that of the emission from crystal A.

The slope of the PYC of crystal B near the threshold energy ($h\nu$ = 5.9 - 6.1 eV) changes appreciably compared with that of crystal A. Furthermore, the PYC of crystal B exhibits deep troughs (Fig. 4(a), e′ and f′). Troughs e′ and f′ do not correspond to the minima of the absorbance but to maxima denoted by the arrows pointing upwards in Fig. 4(b). However, the troughs in the PYC of crystal A (Fig. 3(a), f, g and h) are very shallow and the photon energies corresponding to them coincide closely with those of the absorbance minima in Fig. 3(b).

The threshold energy can be determined using the following power law relation reported by Kochi *et al.* [5]:

$$Y \propto (h\nu - E_{\mathrm{th}})^m \qquad 5/2 \leqslant m \leqslant 3 \tag{3}$$

where Y is the quantum yield of the external photoelectrons, $h\nu$ is the photon energy of the incident light and E_{th} is the threshold energy of the photoemission. When the power law relation is applied to the data shown in Figs. 3(a) and 4(a) a linear relation is obtained between the quantum yield and the photon energy near the threshold (Fig. 5). Values of m = 5/2 and m = 3 were obtained for crystals A and B respectively. Extrapolation of the lines to the lower energy region of the quantum yield (10^{-7}) yielded values of E_{th} of 6.05 eV and 5.85 eV for crystals A and B respectively.

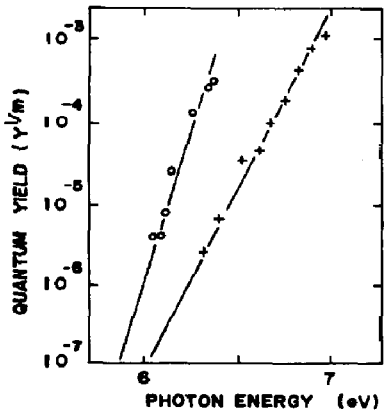

Fig. 5. Power law fit of the photoelectric yield near the threshold energies for crystals A (+) and B (○). The threshold energies E_{th} for crystals A and B are 6.05 eV for m = 5/2 and 5.85 eV for m = 3 respectively.

3.2. Energy distribution curves

Figures 3(c) and 4(c) show the EDCs of crystals A and B respectively. E_B plotted on the abscissa is the binding energy of electrons in the crystal and is measured from the vacuum level. The relation between E_B and E_k is given by

$$E_B = h\nu - E_k \tag{4}$$

A schematic diagram of the electronic energy levels is shown in Fig. 6. The total numbers of emitted photoelectrons obtained by integrating the EDCs shown by broken and full curves in Fig. 3(c) are in the ratio 1:8, and those obtained by integrating the EDCs shown by broken and full curves in Fig. 4(c) are in the ratio 1:18. All the peaks (except f′ and g′) can be attributed to discrete structures in the valence bands [3 - 7, 10]. The binding energies corresponding to each EDC spectrum are listed in Table 1. Peaks b and b′ have not been observed by other workers. Each peak in the EDC spectra shows a gentle slope toward the E_B side as shown in Figs. 3(c) and 4(c). Peaks f and i which appear at $h\nu$ = 7.65 eV and $h\nu$ = 10.25 eV in crystal A

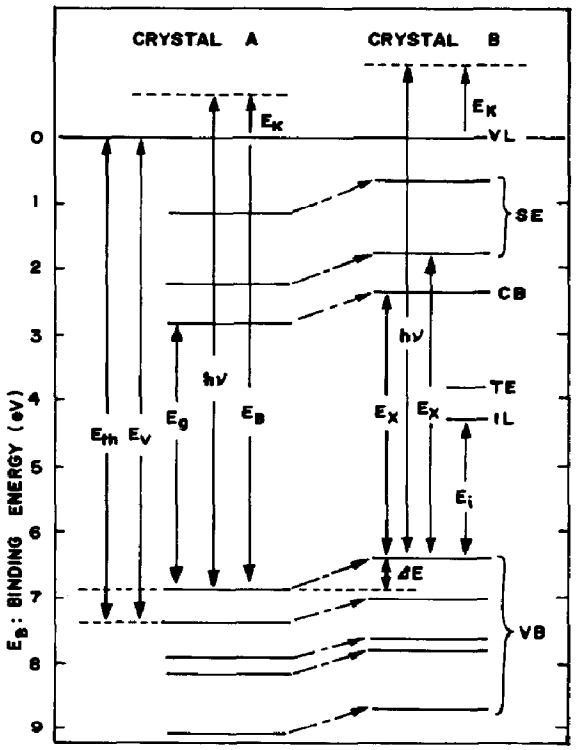

Fig. 6. Schematic energy level diagrams for crystals A and B: VL, vacuum level; SE, singlet exciton levels; TE, triplet exciton levels; CB, conduction band; IL, oxygen impurity level; VB, valence bands; E_k, kinetic energy of the photoelectron; E_V, binding energy of the valence band; $h\nu$, excitation energy; ΔE, difference between the energies of the valence bands of crystals A and B; E_g, band gap energy; E_x, energy of the exciton state; E_i, energy of the impurity state; E_{th}, threshold energy of photoelectrons.

TABLE 1

Energy values of peaks in the EDC of crystals A and B

Crystal A			*Crystal B*				*Literature results for* ΔE_V (eV)		
Peak	E_{VA} (eV)	ΔE_{VA} (eV)	*Peak*	E_{VB} (eV)	ΔE_{VB} (eV)	ΔE_{AB} (eV)	[18]	[7]	[19]
a	0.55	0	a′	0.19	0	0.36	0	0	
b	1.1	0.53	b′	0.80	0.61	0.3			
c	1.6	1.05	c′	1.4	1.21	0.2	1.0	1.05	
d	1.8	1.25	d′	1.6	1.41	0.2	1.25	1.27	1.3
e	2.75	2.20	e′	2.5	2.31	0.25	2.1	2.09	
f	3.5	2.95	f′	3.4	3.21	0.1	3.1		4.1

E_{VA}, E_v value of EDC peaks in crystal A.
E_{VB}, E_v value of EDC peaks in crystal B.
ΔE_{AB}, difference between the E_v values of EDC peaks in crystals A and B ($\Delta E_{AB} = E_{VA} - E_{VB}$).

are low compared with peaks obtained at higher values of E_B. However, peak f′ at $h\nu$ = 10.2 eV in crystal B is the highest of all the peaks obtained at all excitation energies.

Figures 7(a) and 7(b) show the EDC spectra expressed with the kinetic energy E_k obtained using eqn. (4) plotted on the abscissa rather than E_B as in Figs. 3(c) and 4(c). Peak α in Fig. 7(b) corresponds to peaks g′ and k′ in Fig. 4(c) and peak β in Fig. 7(b) corresponds to peaks f′ and j′ in Fig. 4(c). Peaks α and β are located at E_k = 0.45 and at E_k = 0.85 eV respectively, and the peak energies remain constant regardless of the excitation energy. Peaks of this type were not observed in Fig. 7(a).

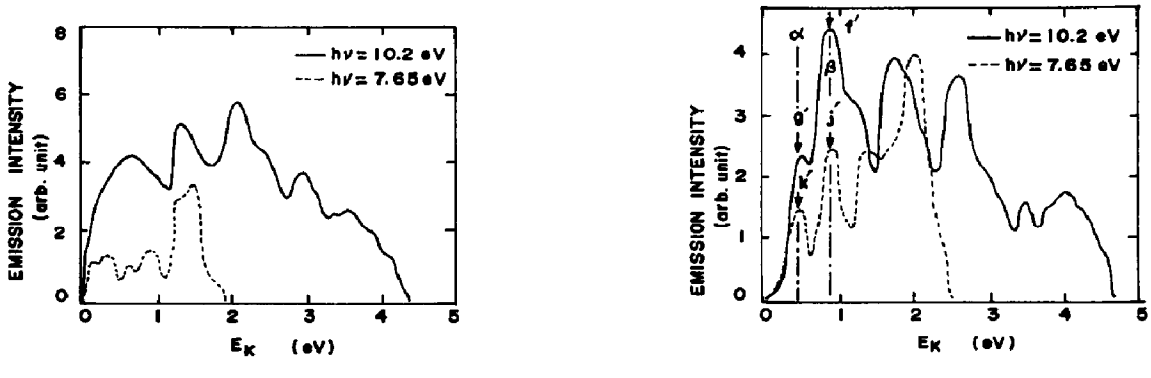

(a) (b)

Fig. 7. EDC spectra expressed with the kinetic energy E_k rather than the binding energy E_B plotted on the abscissa: (a) crystal A; (b) crystal B.

4. Discussion

The photoemission of crystals A and B can be explained in terms of the following electron energy loss processes.

(1) Photoelectrons which are optically excited in a crystal collide with electrons either in the valence bands or in impurity levels. The electrons ejected from the valence bands may be trapped by the impurity levels and the electrons ejected from the impurity levels may relax into the conduction band. The energy of the photoelectrons decreases in both of these processes. We refer to the combination of these mechanisms as the ejection process.

(2) Energy relaxation of the excited electrons takes place by the Auger effect or autoionization. In this case the impurities may affect the energy relaxation process. We refer to this process as the relaxation process.

4.1. Photoelectron ejection process

The origin of the deep troughs e′ and f′ in Fig. 4(a) can be explained in terms of the following photoelectron ejection processes.

Luczak [20] assigned an oxygen impurity state in a *p*-terphenyl single crystal to a *p*-terphenyl–O_2 complex. This impurity energy level is located at 2.1 ± 0.1 eV which is near the middle of the band gap (E_g = 4.0 - 4.3 eV [10, 20]) as shown in Fig. 6.

According to Shida and Hanzaki [21] and Shirakawa *et al.* [19] the intermolecular transition of electrons between hosts (*p*-terphenyl molecules) and guests (*p*-terphenyl–O_2 complexes) can strongly affect the photoemission processes in oxygen-doped crystals. When a photoelectron is optically excited in the crystal, it may collide inelastically with an electron in the valence band which will be ejected and trapped in the impurity level. The photoelectron undergoes an energy loss E_i and creates an exciton together with a hole in the valence band. Thus neither the photoelectron nor the ejected electron is emitted from the vacuum level. The onset energy E_s of the ejection process is given by

$$E_s = E_x + E_i \tag{5}$$

where E_x and E_i are the exciton energy and the impurity level energy respectively (see Fig. 6) (in what follows the energy is measured from the top of the valence band).

Some workers [10, 18, 22] have shown that the creation of excitons makes a large contribution to the ejection process. A photoelectron collides with an impurity and ejects an electron which jumps into the conduction band. The photoelectron undergoes an energy loss $E_g - E_i$ and creates an exciton together with a hole in the valence band. The onset energy E_s' of this ejection process is given by

$$E_s' = E_x + E_g - E_i \tag{6}$$

where E_g is the band gap energy.

The lowest singlet exciton energy of *p*-terphenyl has been estimated to be 4.75 eV above the top of the valence band by internal photoelectric

measurements [10]. Venghaus and Hinz [23] assigned a higher value to the exciton energy (5.75 eV above the top of the valence band) by using energy loss spectra. (We obtained this value by averaging the spectra in the direction of the a and b axes, because the a and b axes are approximately equal to the z and y axes of the anisotropic dielectric tensor.)

When the lowest singlet exciton energy E_x = 4.75 eV [10] and E_i = 2.1 ± 0.1 eV [20] are substituted in eqn. (5), the first onset energy of the ejection process $E_s(1)$ is found to be about 6.9 eV. Similarly, when the higher singlet exciton energy E_x = 5.75 eV is substituted in eqn. (5), the second onset energy $E_s(2)$ is found to be 7.9 eV. When E_g = 4.0 eV [10] and the values of E_x and E_i used above are substituted in eqn. (6), the first and second onset energies $E_s'(1)$ and $E_s'(2)$ are found to be 6.7 eV and 7.7 eV respectively. The quantum yield appears to decrease at 6.9 eV and 7.7 eV (Fig. 4(a), peaks e′ and f′). Since neither the photoelectron nor the ejected electron is emitted from the surface of the crystal at the first and second onset energies of the ejection process, the photoemission disappears. Therefore troughs e′ and f′ may correspond to the first and second onset energies of the ejection process described above. The ejection process described by eqns. (5) and (6) takes place in crystal B.

4.2. Enhancement of photoelectron relaxation processes

In crystal B (Fig. 7(b)) peaks α and β are located at E_k = 0.45 eV and E_k = 0.85 eV respectively and these energies are unchanged regardless of the excitation energy. This result implies that peaks α and β can be attributed to an energy relaxation process such as the Auger effect [24] or autoionization [7, 8] related to the presence of oxygen impurities. Peaks of this type are not observed for crystal A (Fig. 7(a)). We believe that peaks α and β in crystal B are due to an energy relaxation process.

The Auger effect can take place when there are two electrons in an impurity level and one hole in the lower valence band. If a hole is created by the absorption of a high energy photon which has exceeded the threshold energy required for a photoelectron to escape from the crystal and an electron in the impurity level recombines with the hole, the recombination energy will be transferred to another electron in the impurity level, to an electron in the conduction band or to a triplet exciton state. (We did not include the singlet exciton state because the results disagreed with the present data (the EDC spectra).) The kinetic energies E_k corresponding to the peaks α and β are related to the energy of the lower valence band via the conservation of energy. When the recombination energy is transferred to an electron in the impurity level the equation for the conservation of energy is

$$E_i + E_v - E_{th} = E_k + E_{th} - E_i$$

where E_i is the energy of the oxygen impurity level, E_v is the energy of the valence band and E_{th} is the threshold energy of the photoelectron (see Fig. 6). Thus E_v can be written

$$E_v = E_k + 2(E_{th} - E_i) \tag{7}$$

When the recombination energy is transferred to an electron in the conduction band

$$E_i + E_v - E_{th} = E_k + E_{th} - E_c$$

where E_c is the energy of the conduction band. Thus

$$E_v = E_k + 2E_{th} - (E_c + E_i) \quad (8)$$

When the recombination energy is transferred to a triplet exciton state

$$E_i + E_v - E_{th} = E_k + E_{th} - E_t$$

where E_t is the energy of the triplet exciton state. Thus

$$E_v = E_k + 2E_{th} - (E_t + E_i) \quad (9)$$

Next we consider the mechanism of the autoionization process which can be expressed as energy transfer between an exciton state and an oxygen impurity state and consists of the following steps.

(1) A high energy exciton is created optically.

(2) Energy transfer occurs between an electron in the impurity state and the exciton state.

(3) The electron in the impurity state is emitted into a vacuum as a result of the energy transfer. The energy conservation equation for E_k and E_v in this process is the same as that given by eqn. (9) for the Auger process.

In order to find the binding energies of the valence bands relating to these relaxation processes, we attempted to analyse the origins of peaks α and β in the EDC spectra of crystal B. The binding energies of the valence bands were calculated from eqns. (7) - (9) corresponding to the above two relaxation processes by substituting E_{th} = 5.85 eV, E_i = 2.1 eV [20], E_c = 4.0 eV [10] and the energies of peaks α (E_k = 0.45 eV) and β (E_k = 0.85 eV) obtained in our experiments. The results of this analysis are given in Table 2.

TABLE 2

Valence band energies obtained from peaks α and β in the EDC of crystal B by using equations derived for the Auger and autoionization processes

Valence band energy (eV)		*Equation*
From peak α[a]	*From peak* β[a]	
6.05	6.45 (a′)	(8)
7.50 (c′)	7.90 (d′)	(9)
7.95 (d′)	8.35	(7)

[a] The symbols in parentheses indicate peaks assigned from the present EDC data for crystal B.

4.3. Other effects of oxygen molecules on the photoemission process

The difference between the threshold energies of photoemission from crystals A and B, *i.e.* E_{th} (6.05 eV) $- E_{th}'$ (5.85 eV), is 0.20 eV. This differ-

ence can be attributed to the polarization caused by the formation of dipoles of O_2^-–*p*-terphenyl$^+$ complexes in crystal B. It is related to the differences between the polarization energies of crystals A and B [25] and can be attributed to the dipole field of O_2^-–*p*-terphenyl$^+$ complexes which decreases the threshold energy E_{th}'.

Figure 8 shows the EDC spectra of crystals A and B obtained at an excitation energy of 10.2 eV. The values of E_B for the EDC peaks in crystal B are 0.19 - 0.45 eV lower than the corresponding peaks in crystal A (see Table 1). The differences $\Delta E = E_B - E_B'$ between the binding energies corresponding to the EDC peaks are listed in Table 1. They decrease with increasing E_B.

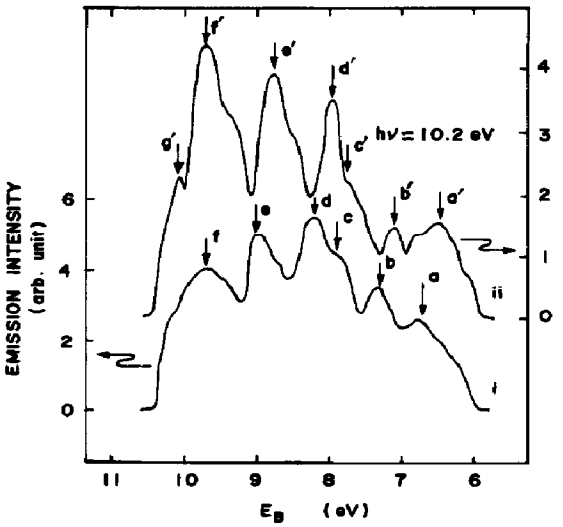

Fig. 8. EDC spectra of crystals A (curve i) and B (curve ii) at an excitation energy of 10.2 eV. Each peak in crystal B lies at a lower value of E_B (ΔE = 0.19 - 0.45 eV) than that of the corresponding peak in crystal A (see Table 1).

The quantum yield of photoelectrons emitted from the surface of crystal B is a factor of 100 less than that of the emission from crystal A. This result can be attributed to a change in the potential barrier owing to the presence of doped oxygen impurities near the crystal surface.

5. Conclusion

We measured the photoemission spectra of oxygen-doped *p*-terphenyl single crystals and found new peaks α and β in the EDC spectra. We propose that the new peaks can be assigned to the relaxation of photoelectrons caused by the presence of the oxygen impurity.

Acknowledgments

We are grateful to Professor M. Tomura for his comments. We should like to thank Mr. K. Kakumoto for his help with the calculations and Mr. Y. Kashiwagi for his advice concerning the experiments.

References

1 W. E. Spicer, in F. Abèles (ed.), *Optical Properties of Solids*, North-Holland, Amsterdam, 1972, pp. 755 - 858.
2 J. W. Rabalais, *Principles of Ultraviolet Photoelectron Spectroscopy*, Wiley, New York, 1977.
3 L. E. Lyons and G. C. Morris, *J. Chem. Soc.*, (1960) 5192.
4 F. I. Vilesov, A. A. Zagrubski and D. S. Garbusov, *Fiz. Tverd. Tela, 5* (1963) 2000.
5 M. Kochi, Y. Harada and H. Inokuchi, *Bull. Chem. Soc. Jpn., 40* (1967) 531.
6 S. Hino, K. Seki and H. Inokuchi, *Chem. Phys. Lett., 36* (1975) 335.
7 N. Geacintov and M. Pope, *J. Chem. Phys., 50* (1969) 814.
8 A. A. Zagrubskii and F. I. Viesov, *Fiz. Tverd. Tela, 13* (1971) 2300.
9 M. Kochi, Y. Harada, T. Hirooka and H. Inokuchi, *Bull. Chem. Soc. Jpn., 43* (1970) 2590.
10 K. Seki, T. Hirooka, Y. Kamura and H. Inokuchi, *Bull. Chem. Soc. Jpn., 49* (1976) 904.
11 N. Ueno, A. Okazaki, Y. Hayasi and S. Kiyono, *Chem. Phys. Lett., 42* (1976) 119.
12 R. G. Newburgh, L. H. Heroux and H. E. Hinteregger, *Appl. Opt., 1* (1962) 733.
13 F. Masuda, *Sci. Light, 14* (1965) 147.
14 R. Allison, J. Burns and A. J. Tuzzolino, *J. Opt. Soc. Am., 54* (1964) 1381.
15 J. A. R. Samson, *J. Opt. Soc. Am., 54* (1964) 6.
16 W. F. Krolikowski, *Ph.D. Thesis*, Stanford University, 1967.
17 L. W. James, R. C. Eden, J. L. Moll and W. E. Spicer, *Phys. Rev., 174* (1968) 909.
18 P. B. Merkel and W. H. Hamill, *J. Chem. Phys., 66* (1971) 1409.
19 A. Shirakawa, K. Nakagawa and N. Itoh, *Mol. Cryst. Liq. Cryst., 44* (1978) 211.
20 F. J. Luczak, *Ph.D. Thesis*, Boston College, 1972.
21 T. Shida and I. Hanzaki, *Bull. Chem. Soc. Jpn., 43* (1970) 646.
22 S. Choi, J. Jortner, S. A. Rice and R. Silvey, *J. Chem. Phys., 41* (1964) 3294.
23 H. Venghaus and H. J. Hinz, *J. Chem. Phys., 62* (1975) 4737.
24 J. I. Pankove, *Top. Appl. Phys., 17* (1977) 6.
25 H. Meier, in H. F. Ebel (ed.), *Organic Semiconductors, Monogr. Mod. Chem., 2* (1974) 284.